INVESTIGATION OF IMPACT RESPONSE OF 2D BIAXIAL BRAIDED COMPOSITES WITH HYBRID CONFIGURATION USING MICRO-CT

E. Bond[1], and G. W. Melenka[2*]

[1] School of Mechanical and Aerospace Engineering, Queen's University Belfast, Northern Ireland (ebond04@qub.ac.uk)

[2*] Department of Mechanical Engineering, Lassonde School of Engineering, Toronto, Canada
*Corresponding author (gmelenka@yorku.ca)

Keywords: Braided Composite, Charpy Impact, Micro-Computed Tomography

ABSTRACT

Braided composites formed from the embedding of woven fibres in a matrix boast favourable mechanical properties and overall damage resistance. Variation and control of the fibre/ matrix composition and layup configuration allow for a degree of tailoring with regard to the mechanical properties and overall damage resistance. This work aims to investigate the low-velocity impact response of carbon-aramid/epoxy 2D biaxial braided composites in a hybrid layup configuration using micro-computed tomography (micro-CT). A multi-step procedure is utilised whereby samples are impacted via a Charpy impact test rig before further assessment and analysis through micro-CT, and image visualisation and analysis software. Impact testing via a Charpy test rig allows for the initiation of damage within a controlled experimental environment. Micro-CT allows for the analysis and further assessment of damage within braided composites, including but not limited to damage resistance and damage progression. The multi-step assessment and analysis focused on throughout this work allow for the comparison of differing layup methods of 2D bi-axially braided composites as well as highlighting the cruciality of non-destructive (ND) analysis of impact-tested samples. Initial investigation of impact response behaviour in 2D braided hybrid composites will form a basis for progressive fatigue response behaviour and increased application.

1 INTRODUCTION

Braided composites are formed from "woven fibres embedded in a matrix" [1], and are generally categorised as 2D or 3D. 2D braids are further classified into biaxial and triaxial configurations with each classification having a distinguishable pattern: Diamond, Regular, or Hercules [2]. While biaxial or triaxial configuration and pattern type are significant in the properties of the 2D braided composite, the braid angle also strongly influences braid mechanical properties; with a low braid angle providing greater axial contribution [3], and a higher braid angle seeing improved transverse elastic modulus [4].

2D braided composites have continuously increased in utilisation largely due to their favourable mechanical properties and overall damage resistance compared to standard laminated composites [1]. Seeing uses across a range of industries, some common uses of 2D braided composites include over-braided fuel lines, catheters, and aircraft structural parts [5]. With regards to impact damage resistance, 2D braided composites see beneficial applications in sporting equipment [5], aircraft engine casings [6], and fan blades [7].

Aramid, a type of synthetic fibre composition, consists of long-chain synthetic polyamides that provide high tensile strength and impact resistance [8]. Aramid fibres can be classified into two main types: meta-aramid and para-aramid, with meta-aramid seeing applications in the likes of thermal and/or radiation resistance or fire-retardant textiles, and para-aramid seeing applications in the likes of fibre reinforced plastics, or stress skin panels [8]. This study sees the use of a para-aramid 2D braid.

Consisting of carbon atoms bonded together to form an organic, low-weight, high stiffness composition [9] carbon fibre similar to aramid, sees uses in a plethora of applications from wind turbines to high-end cars [10]. Along with an impact-resistant para-aramid 2D braid, a high-stiffness 2D carbon fibre braid is utilised to create a hybrid braid suitable for investigation of impact response. Regarding the impact/ damage response of 2D braided composites, Charpy impact tests are commonly utilised in experimental testing and assessment and will form the basis of testing in this study [11].

Damage within braided composites including impact response and damage progression can be analysed and further assessed through techniques such as micro-computed tomography (micro-CT) [12], infrared thermography [12], and digital image correlation [12]. While each method has advantages, micro-CT often remains preferable regarding non-destructive (ND) analysis as it allows 2D surface measurement and analysis of internal deformation of damage progression [12].

Current studies regarding 2D braided composites have used the ultrasonic c-scan method in the investigation of low-velocity impact response in carbon-aramid/ epoxy hybrid and several investigations into medium and high-velocity impact in glass-carbon hybrids [11]. The study by Sun *et al.* [11] evaluated the effects of hybridisation using aramid fibre to reinforce carbon/epoxy composites through c-scan analysis. The effects on impact properties including ductility index (DI), Pm (peak load), and internal damage of four hybrid variations were produced and tested including interply hybrid (IE), sandwich-like hybrid (SA), unsymmetric hybrid (US), and intraply hybrid (IA) were analysed. It was found on c-scans that SA and US displayed severe delamination while IA and IE displayed greater internal damage than visible external damage.

At present, no publications could be found on the use of micro-CT to investigate impact response within 2D braided composites which leaves scope for investigation. Based on current studies, this work aims to investigate the low-velocity impact response of carbon-aramid/epoxy 2D biaxial braided composites in a hybrid layup configuration through micro-CT. With the outlined aim, this work will include the manufacture of 2D braided composites with a hybrid configuration via vacuum bagging before Charpy impact testing. To investigate the impact response, samples will then be scanned using the Micro-CT process before scan analysis via reconstruction software and subsequent pore analysis. This work will lead to a better understanding of the low-velocity impact behaviour of hybrid biaxial braided composite structures.

2 METHODS

2.1 MANUFACTURE OF BRAIDED COMPOSITES

The pattern of the braid can be classified as Diamond (1x1), Regular (2x2), or Hercules (3x3). Both samples used in this study were fabricated in the Regular braiding configuration. Initial 2D braided composite specimens were manufactured using aramid (50.8 mm (2″), 9.9 oz./sq yd, 0.018″ Thick, FibreGlast Developments CORP, Brookville, Ohio) and carbon fibre biaxial sleeves (50.8 mm (2″), 36.8 ft/lb, 254 GSM (7.5 oz/sq yd), 0.011 in, TR30S 3 K, A&P Technologies, Cincinnati, Ohio).

Both braided sleeves were cut into three 180mm x 50.8mm strips before layup in configurations identified as Aramid/Carbon/Aramid Layered Laminate (A/C/A-LL), and Carbon/Aramid/Carbon Layered Laminate (C/A/C-LL). Table 1 details the identification code and the corresponding number of layers as well as the material order.

Table 1: Specimen identification and corresponding layup configuration

Identification Code	Layup Configuration	No. of Layers	Cross-sectional layer order
A/C/A-LL	Layered Laminate	3	Aramid Carbon fibre Aramid
C/A/C-LL	Layered Laminate	3	Carbon fibre Aramid Carbon fibre

LL is achieved by stacking fibre braids atop one another, creating three distinct layers as shown in Figure 1 (b). A cross-section schematic of the LL configuration is shown in Figure 1(a), where the pattern indicates the opposite material choice to white fill.

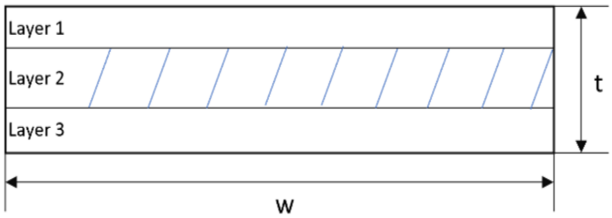

(a)

(b)

Figure 1: Schematic of Internal Layup of Layered Laminate (LL)

During the layup process, the 235 x 235 x 3mm borosilicate glass vacuum plate was cleaned with a thin coat of acetone (CAS #67-64-1, Acetone (Certified ACS), Fisher Scientific, 81 Wyman Street, Waltham, MA). Following the drying of the acetone, the plate was coated with a thin, even layer of releasing agent (700-NC, Loctite Frekote, Henkel AG & Co. KGaA, Dusseldorf, Germany).

All specimens were impregnated with a two-part epoxy (#2000 epoxy resin, Fibre Glast Developments CORP, Brookville, Ohio) and hardener (#2060 epoxy hardener, Fibre Glast, Developments CORP, Brookville, Ohio), mixed in a 100:27 ratio, respectively. After ensuring specimens were evenly impregnated with resin, they were placed in a vacuum bag as shown in Figure 2 (a), and then left for 24 hours for curing. Following completion of the initial layup, each specimen was cut via Flow Mach 2b water jet cutter into three samples (I, II, and III, from left to right) of dimensions approx. 127mm x 10mm x 2.5mm, as shown in Figure 2 (b).

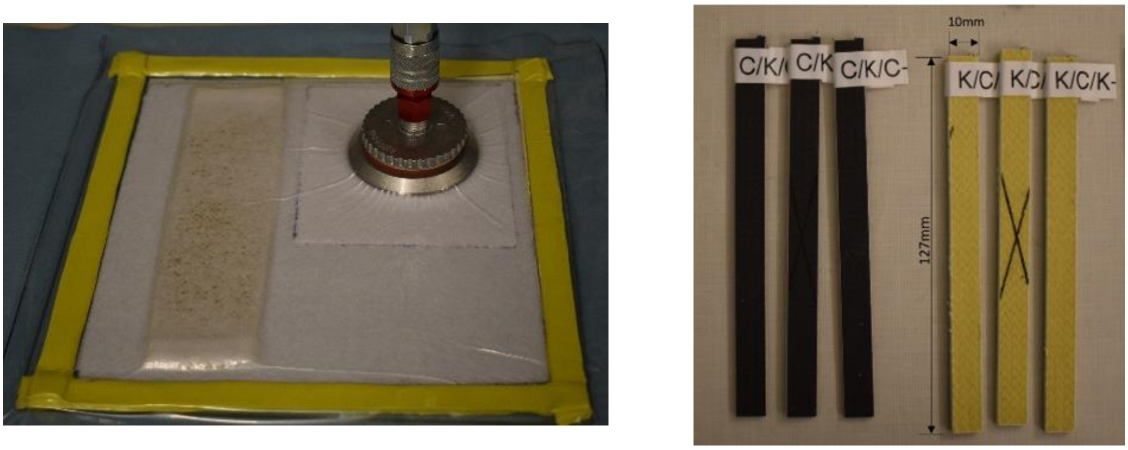

(a) (b)

Figure 2: Braided specimen manufacturing, (a) Braded specimen in Vacuum Bag. (b) Specimens post-water jet cutting with standard dimension (127mm x 10mm x 2.5mm)

2.1.1 SPECIMEN AND SAMPLE PROPERTIES

Due to its influence on how the braid performs during testing, the braid angle was determined for each specimen before cutting. Due to variations in the braid angle across the specimen/ sample due to the manufacturing process and human error in measurements, an average of eight measurements were taken across the length and width of the specimen using a digital protractor (ImageJ, Research Services Branch, National Institute of Mental Health, Bethesda, Maryland, USA) on images taken at 90 ˚to the sample, taken using a digital camera (Nikon D3500 DSLR Camera, 24.2 MP Sensor, NIKKOR 18-55mm f/3.5-5.6G VR Lens, Nikon Canada Inc., 1366 Aerowood Drive, Mississauga, ON).

Using a caliper (Mastercraft Digital Caliper with LCD Display, 6 in (15cm)) the width of each sample was also determined for input parameters for Charpy tests as shown in Table 2. Sample thicknesses shown in Table 5 were calculated through image pixel size measurement and conversion. Figure 1 (b) shows a reference photo taken using a digital microscope (Elikliv EDM4S Coin Microscope, 4.3" 1000x LCD digital screen, Shenzhen, Guangdong, China) perpendicular to the sample that was then used in a basic graphics software (ImageJ, Research Services Branch, National Institute of Mental Health, Bethesda, Maryland, USA) to calculate the pixel length and subsequently the individual layer thicknesses. The material properties of the manufactured samples were estimated using a Classical Laminate Plate Theory (CLPT) property determination software (The Laminator, Version 3.8, Michael Lindell).

2.2 CHARPY IMPACT TEST OF 2D BRAIDED COMPOSITES

Following specimen manufacturing, experimental investigation of A/C/A-LL-II and C/A/C-LL-II samples was conducted using the Charpy test rig (Instron-Ceast-Model-9050, Norwood, Massachusetts) to assess the impact damage resistance and compare the two sample configurations. For this study, the aim was to initiate damage within samples rather than achieve failure of the sample. As per ASTM/D6110, the test configuration consisted of a 10.8J hammer angled at 150 degrees delivering an impact speed of 3.46 m/s [13]. While the width and thickness of each sample deviate from the standard, the length of 127mm complies with ASTM/D6110 [13].

Prior to testing, the centre point of each sample was measured and marked to allow alignment in the Charpy test rig. Due to the thin composite nature of the samples as well as the focus being on the initiation of damage rather than breaking a notch was not utilised. To maintain an upright position in the shoulder, the samples were supported but not restricted with the use of tape as shown in Figure 3. Following the securing of samples in the test rig, the parameters stated in Table 2 were inputted before commencing testing.

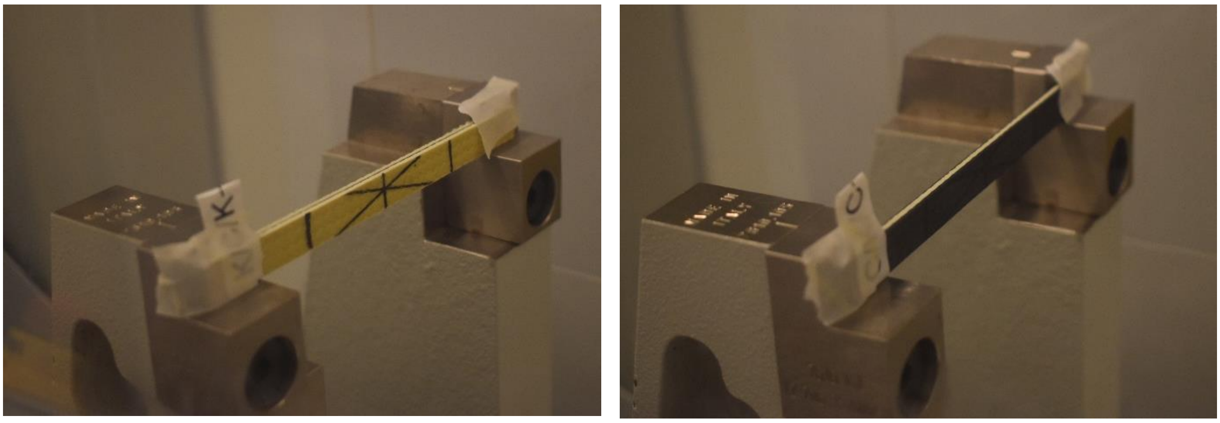

(a) (b)

Figure 3: Samples in-situ Charpy Impact Test, (a) Sample lay-up with outer aramid layer A/C/A- LL, (b) Sample lay-up with outer carbon fibre layer C/A/C- LL

Table 2: Charpy impact test rig inputs

Parameter Type	**Value**
Angle	150.00°
Hammer	7600.110 Charpy ASTM – 10.8J
Parameters Set	ASTM6110
A/C/A-LL Sample Width	10.3mm
C/A/C- LL Sample Width	10.2mm

2.3 MICRO-CT OF 2D BRAIDED COMPOSITES

Following impact, test samples were cut to a size of 60mm x 10mm x 2.5mm to comply with the maximum dimensions of the micro-CT scanner (SkyScan 1272 microtomograph, Bruker-MicroCT, Kontich, Belgium). Samples were situated in a fixture in the micro-CT chamber as shown in Figure 4 to maintain sample orientation and reduce the likelihood of distorted images.

Each sample was scanned with an accelerating X-ray source voltage of 50kV and a current of 153µA with an Al 0.25mm filter. A total of 1800 projections were taken through 360°rotation (rotation step = 0.2°) with 2x2 binning and 4.5 µm pixel size. Similar scan settings have been used for analysing 2-D tubular braided composites by Gholami *et al.,* highlighting that a smaller step size leads to more accurate results [14].

Each scan had a field of view of 11.034mm x 11.034 mm x 0.720mm. Samples were also elevated by 24mm to ensure the field of view contained the damaged area of the sample. X-ray projections were processed via reconstruction software (NRecon V1.7.1.0, Allentown, Pennsylvania) with post-alignment -10.50 and smoothing of 2 (gaussian). A ring artifact correction of 10 was also used due to imperfections in the micro-CT detector elements causing concentric-ring artifacts (ring artifacts) that disturbed image quality, as demonstrated in work by Kyriakou *et al.* [15].

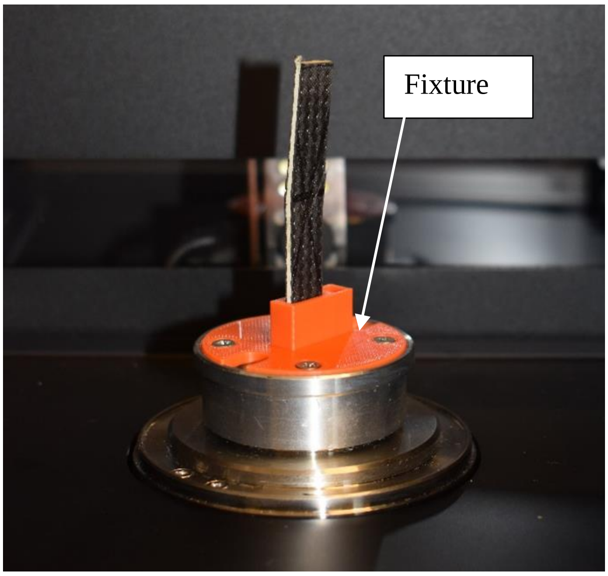

(a)

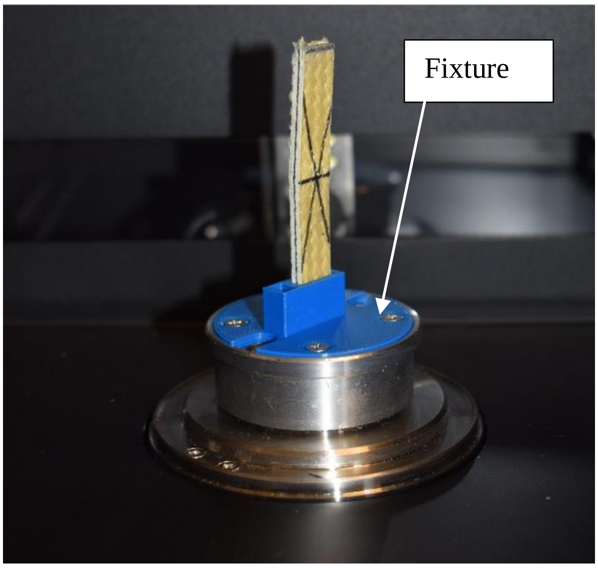

(b)

Figure 4: Sample in CT Scanner, (a) Sample C/A/C- LL in an orange 3D printed fixture, (b) Sample A/C/A- LL in a blue 3D printed fixture

Image visualisation and analysis software (CTan 1.16.90, Bruker microCT, Belgium) allowed initial qualitative analysis and scan size determination. To allow for quantification, scan images were reduced into a region of interest (R.o.I) of 4.75mm x 4.41mm, as shown in Figure 5 (a) and Figure 5 (b), to ensure porosity was not overestimated. Images were then binarized, as shown in Figure 5 (c) and Figure 5 (d), prior to custom processing in the following order: threshold, de-speckle, and 3D analysis, where 3D analysis is a tool within the CTan software that allows calculation of multiple selected parameters such as porosity, and geometry. The thresholding process used a lower grey threshold of 25 and an upper grey threshold of 255. At certain locations, image noise can occur because of a low number of photons being present [16] causing disturbed image quality. Therefore, to reduce disturbance, de-speckling was used to filter white speckles less than 10 voxels. Following despeckling, the ‘3D analysis’ tool within CTan was utilised to quantify the porosity including the number of open and closed pores, open and closed porosity, and total porosity.

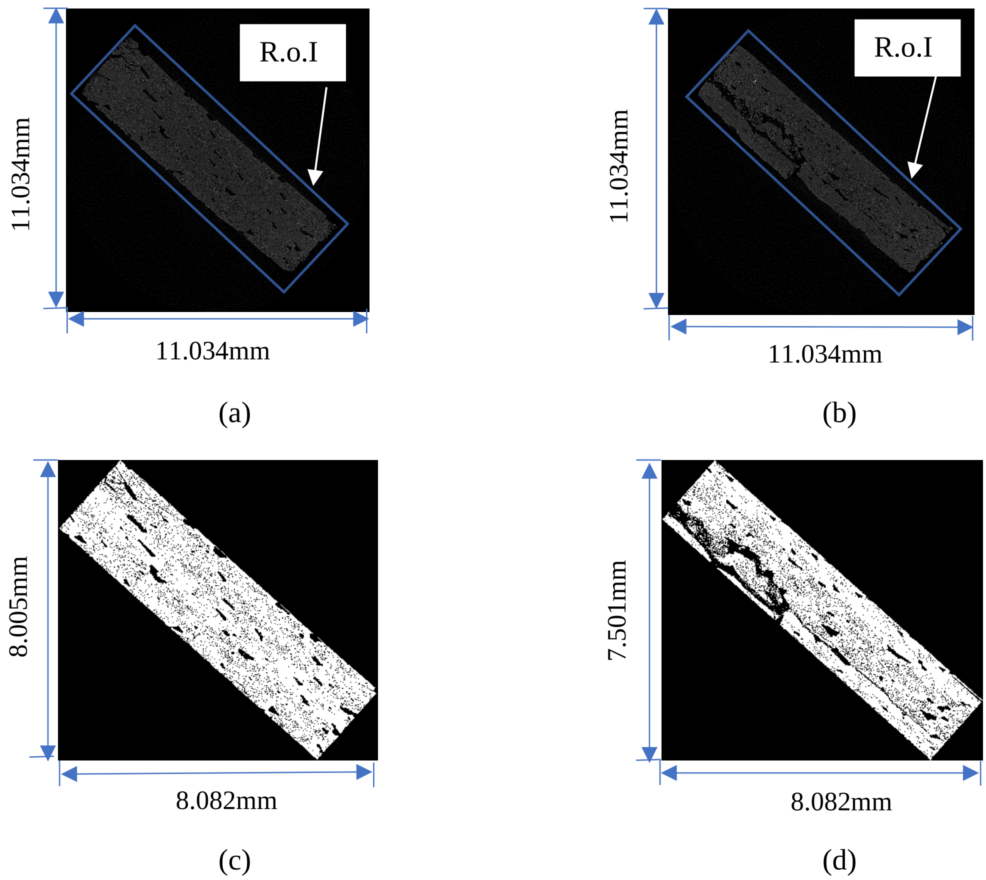

Figure 5: Images of post-reconstruction analysis stages, (a) A/C/A- LL initial reconstruction, (b) C/A/C- LL initial reconstruction, (c) A/C/A- LL binarized image, (d) C/A/C- LL binarized image

3 RESULTS AND DISCUSSION

3.1 SPECIMEN AND SAMPLE PROPERTIES

As discussed in Section 2.1.1, Table 3 highlights the measured braid angles, calculated mean, and standard deviation for specimens, prior to water jet cutting. The variation in the braid angle across specimens and samples is consistent within 2° of each other.

Table 3: Specimen braid angles

Specimen	Braid Angle (degrees)									
	1	2	3	4	5	6	7	8	Mean	Standard Deviation
A/C/A-LL	33.5	31.2	29.6	28.7	30.5	31.8	30.4	32.6	31.0	1.47
C/A/C-LL	31.8	29.2	31.9	29.8	28.1	30.3	31.5	30.6	30.4	1.25

Table 4 details the sample's thicknesses as discussed in Section 2.1.1 which formed inputs for the Charpy impact test as well as the prediction of material properties.

Table 4: Measured Sample Thicknesses

Sample Configuration	Measured Thickness (mm)		
	Carbon Layer	Aramid Layer	Total
A/C/A-LL	0.419	1.091	2.601
C/A/C-LL	0.522	1.055	2.099

Material properties were calculated for each specimen shown in Table 5 using the calculated braid angle, the determined number of layers (3 or 5), and the measured layer thicknesses. The apparent material properties allowed a prediction of which sample layup was likely to perform the worst in terms of the likelihood of damage to be present.

The determination of braid angles allowed for the apparent sample properties to be estimated as shown in Table 5 and subsequently predict which configuration will demonstrate a greater impact response. A/C/A-LL has an apparent extensional modulus in the x-direction and y-direction that's, respectively, 6.60% and 25.35% greater than the C/A/C-LL apparent extensional moduli. This means that the A/C/A-LL configuration should display a greater impact response, making it less likely to show signs of damage compared to C/A/C-LL.

Table 5: Estimated Material Properties

Sample	Apparent Extensional Modulus, E [Pa]	
	EX	EY
A/C/A-LL	1.470e+6	1.087e+6
C/A/C-LL	1.379e+6	8.672e+5

3.2 CHARPY IMPACT TEST

The resulting energy absorption (absolute energy) for C/A/C-LL-II and A/C/A-LL-II samples were 3.167J (29.32%) and 4.164J (38.55%), respectively as detailed in Table 6.

Table 6: Resulting energy from Charpy Impact tests

Sample	Absolute Energy (%)	Energy (J)
A/C/A-LL-II	38.55	4.164
C/A/C-LL-II	29.32	3.167

Visual inspection showed significant permanent deformation in both samples with C/A/C-LL-II showing a visible surface crack that can be identified in Figure 5 (b): C/A/C-LL-II scan reconstruction. The results show, as predicted, that the primarily aramid sample demonstrated greater resistance to impact than the primarily carbon sample.

From an observational perspective, both samples as shown in Figure 6 (a) were deformed following impact, with the C/A/C-LL-II sample showing a visible 45° crack on the surface as shown in Figure 6 (b).

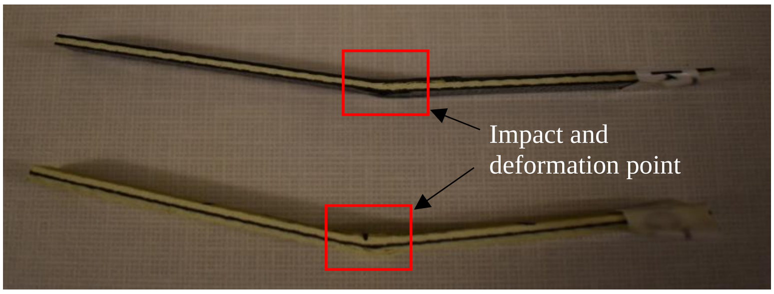

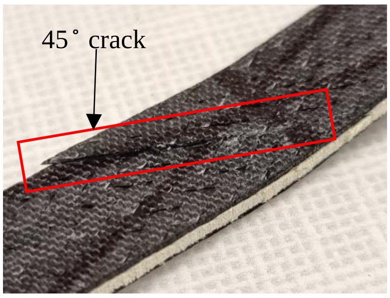

(a) (b)

Figure 6: Impact damage on samples following Charpy Impact, (a) Cross-sectional view showing impact and deformation point, (b) 45 ˚crack on the surface of C/A/C- LL sample.

3.3 MICRO-CT SCAN ANALYSIS

Following the completion of 3D analysis as discussed in Section 2.3, a variety of parameters such as object volume, area moment of inertia, and centroid were determined. The '3D analysis' tool in CTan also allowed pore distribution to be determined, specifically open and closed porosity. As shown in Figure 7 (a) open pores are typically connected to the 'outside' whereas closed pores are independent as shown in Figure 7 (b).

(a)

(b)

Figure 7: Reference of pore types, (a) Open Pore, (b) Closed Pore

Pore distribution throughout both C/A/C-LL and A/C/A-LL samples was examined, namely the closed porosity as shown in Figure 8 (a). Closed porosity is of greater significance during this study due to the fact that the open porosity value was not an accurate representation of the open porosity due to the presence of a crack, as shown in Figure 8 (b).

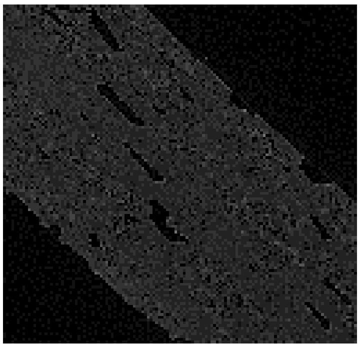

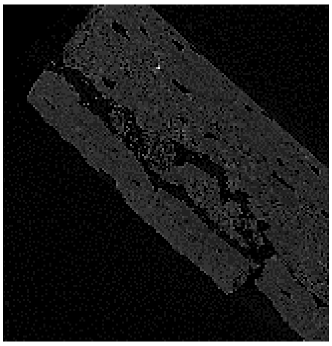

(a) (b)

Figure 8: Resulting image for uCT analysis, (a) Examples of Closed pores, (b) Examples of open pores from the developed crack.

Table 7 summarises the number of closed pores, volume of closed, closed porosity percent, and total porosity for both the A/C/A-LL and C/A/C-LL samples. Table 7 highlights that A/C/A-LL has nearly twice the number of closed pores compared to C/A/C-LL. However, C/A/C-LL has a greater open porosity percent compared to A/C/A-LL which means that failure initiation sites are more likely to develop within C/A/C-LL as highlighted in work by Melenka *et al* [17]. The presence of large open pores indicates the large cracks that have formed because of the impact damage to the test samples.

Table 7: 3D Scan analysis results

Sample	Number of Closed Pores	Volume of Closed Pores (mm^3)	Closed porosity (%)	Open Porosity (%)	Total Porosity (%)
A/C/A-LL-II	1178061	4.71	3.58	13.5	16.6
C/A/C-LL-II	592697	2.43	2.61	21.1	23.2

CONCLUSIONS

2D biaxial braided composites with hybrid configuration were manufactured using aramid/carbon fibre in a layered laminate (LL) to give A/C/A-LL and C/A/C-LL layup configurations. Braid angle, along with thickness measurement of sample layers, allowed for the estimation of material properties, namely apparent extensional moduli in the X and Y. C/A/C-LL appeared to have an apparent extensional modulus of 1.379e+6 (X) and 8.672e+5 (Y), with A/C/A-LL having an apparent extensional modulus of 1.470e+6 (X) and 1.087e+6 (Y). The estimated material properties indicated that the C/A/C-LL is more likely to display a weaker impact response and show damage when compared to A/C/A-LL.

Following manufacture and material property determination, samples were impacted with the commonly utilised experimental testing method of Charpy impact testing. The resulting energy absorption for A/C/A-LL-II and C/A/C-LL-II was 4.164J and 3.167J, respectively, indicating that C/A/C-LL-II had a weaker impact response as previously estimated with apparent material properties. While both samples showed deformation, further visual inspection indicated that C/A/C-LL had a weaker impact response and was more likely to display failure due to the presence of a 45°crack on the surface of the sample.

Due to its ability to analyse internal deformation of damage, high-resolution micro-CT was used to examine the samples as well as quantify the porosity volume, porosity percent, and total porosity. A/C/A-LL-II had a higher closed porosity percent at 3.58% compared to 2.61% for C/A/C-LL-II. However, C/A/C-LL-II had a higher open porosity percent at 21.1% compared to A/C/A-LL-II with an open porosity of 13.5%, meaning that C/K/C-LL-II had a higher chance of failure initiation at open pore sights. This quantification further supports the results of the estimated material properties, Charpy impact tests, and visual inspection in that C/A/C-LL has demonstrated a weaker impact response consistently when compared to A/C/A-LL.

The methods used and discussed in this study allow for an increased understanding of the manufacture and impact response of 2D braided hybrid composites. This study also highlights the cruciality of micro-CT in supporting ND analysis of impact test samples and remains valuable in confirming visual inspection results. With regard to further investigation, a progressive fatigue study following impact would be beneficial in further increasing the understanding of the impact response behaviour of 2D braided composites as well as allowing increased confidence in diversifying the application of 2D braided hybrid composites across industries and components.

ACKNOWLEDGEMENTS

Funding for this work was supported by the Natural Sciences and Engineering Research Council (NSERC) Canada RGPIN-2018-05899 and the MITACs Globalink program.

REFERENCES

[1] G.W Melenka and A. Gholami "Fiber identification of braided composites using micro-computer tomography". *Composites Communications*, Vol 27, 2021
[2] G. W. Melenka et al., "*3 - Manufacturing processes for braided composite materials*," Handbook of Advances in Braided Composite Materials, Elsevier Ltd, 2017, pp. 47–153.
[3] S. Omeroglu, The effect of braiding parameters on the mechanical properties of braided ropes. *Fibres and Textiles in Eastern Europe*. 14. 2006, pp. 53-57.
[4] J.H. Byun, 'The analytical characterization of 2-D braided textile composites', *Composites Science and Technology*, 60(5), 2000, pp. 705-716.
[5] L.R. Sanders, Braiding – a mechanical means of composite fabrication. *SAMPE Q*, 8(2), 1977, pp. 38–44
[6] L.M. Amoo, On the design and structural analysis of jet engine fan blade structures, *Progress in Aerospace Sciences*, 60, 2013, pp. 1–11.
[7] T. Kermanidis, G. Labeas, M. Sunaric, et al. Development and validation of a novel bird strike resistant composite leading edge structure, Applied Composite Materials, 12(6), 2005, pp. 327–53.
[8] M. I. Anjum, Aramid Fibers- An Overview, 2015, *https://textilelearner.net/aramid-fibers-types-properties-manufacturing-process-and-applications/*
[9] P. Bhatt, and A. Goe, 'Carbon Fibres: Production, Properties and Potential Use', *Material Science and Research India*, 14(1), 2017, pp. 52-57.
[10] T. Johnson, *Uses of Carbon Fiber*, 2018 Available at: *https://www.thoughtco.com/uses-of-carbon-fiber-820394*
[11] Y. Sun, SQ. Tian, MY. Tang and D. Chen "Low velocity impact response of carbon-aramid/epoxy hybrid 2D braided composites". *Journal of Tianjin Polytechnic University*, Vol 37, 2018, pp. 1-6
[12] X. Liu, D. Zhang, C. Mao, X. Wang and K. Qian "Full-field progressive fatigue damage of 3D5D braided composites with yarn-reduction: visualization, classification, and quantification". *Composites Science and Technology*, Vol 218, 2022
[13] ASTM Standard D6110. Determination of Charpy Impact Properties.
[14] A. Gholami and G. W. Melenka, "Finite element analysis of 2-D tubular braided composite based on geometrical models to study mechanical performances models to study mechanical performances," *Mech. Adv. Mater. Struct.*, vol. 0, no. 0, pp. 1–17, 2021, doi: 10.1080/15376494.2021.2001879.
[15] Y. Kyriakou, D. Prell, and W. A. Kalender, 'Ring artifact correction for high-resolution micro CT', *Physics in Medicine and Biology*, 54(17), 2009, pp. 385-391.
[16] F. E. Boas, and D. Fleischmann, CT artifacts: causes and reduction techniques. *Imaging Med*, 4, 2012 pp. 229–240.
[17] G. W. Melenka, B. M. Bruni-Bossio, C. Ayranci, and J. P. Carey, 'Examination of voids and geometry of bio-based braided composite structures', *IOP Conference Series: Materials Science and Engineering*, 306(), 2018